Clean Energy, 2020, Vol. 4, No. 2, 120–131

doi: 10.1093/ce/zkaa003
Advance Access Publication Date: 1 April 2020
Homepage: https://academic.oup.com/ce

Research Article

Investigation of adsorption/desorption performance by aminopropyltriethoxysilane grafted onto different mesoporous silica for post-combustion CO_2 capture

Pailin Muchan[1,2], Chintana Saiwan[1,2] and Manit Nithitanakul[1,2,*]

[1]The Petroleum and Petrochemical College, Chulalongkorn University, Soi Chula 12, Phyathai Road, Pathumwan, Bangkok 10330, Thailand
[2]Center of Excellence on Petrochemical and Materials Technology, Chulalongkorn University, Bangkok 10330, Thailand

*Corresponding author. E-mail: Manit.n@chula.ac.th

Abstract

Mesoporous silicas with hexagonal structure (MCM-41 and SBA-15) and cubical interconnected pore structure (KIT-6) were synthesized and modified with aminopropyltriethoxysilane (APTES) for using as adsorbents in carbon-dioxide (CO_2)-adsorption application. The CO_2-adsorption experiment was carried out at room temperature and atmospheric pressure using 15% CO_2 with a flow rate of 20 mL/min and the desorption experiment was carried out at 100°C under N_2 balance with a flow rate of 20 mL/min. The adsorption capacity and adsorption rate of all modified mesoporous silicas were enhanced due to the presence of primary amine in the structure, which was able to form a fast chemical reaction with CO_2. All adsorbents showed good adsorption performance stability after using over five adsorption/desorption cycles. Due to the effect of the adsorbents' porous structure on the adsorption/desorption process, an adsorbent with sufficient pore-size diameter and pore volume together with interconnected pore, KIT-6, represents a promising adsorbent that gave the optimum adsorption/desorption performance among others. It showed reasonable adsorption capacity with a high rate of adsorption. In addition, it could also be regenerated with 99.72% efficiency using 12.07 kJ/mmolCO_2 of heat duty for regeneration.

Received: 5 November 2019; **Accepted:** 4 March 2020

Graphical Abstract

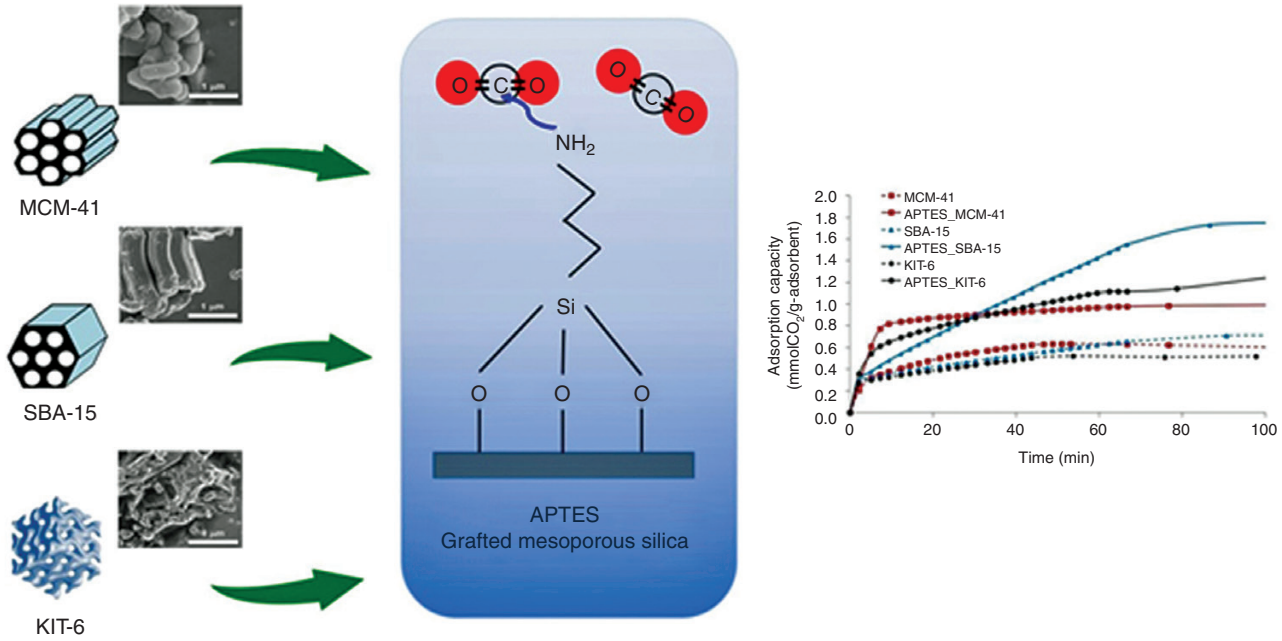

Keywords: CO_2 adsorption; mesoporous silica; adsorption capacity; adsorption rate; heat duty for adsorbent regeneration

Introduction

Fossil fuel is the main source of energy for humans. In this energy-production process of combustion, carbon dioxide (CO_2) is released as a by-product responsible for almost 60% of global warming [1, 2]. In 2018, the global CO_2 emission from fossil fuels and industry was projected to reach 37.1 billion tons [3]. In order to minimize this crisis, CO_2 separation after the post-combustion of fuel is necessary to be applied for minimizing the amount of CO_2 from large emission-point sources. A CO_2-absorption technique using aqueous amine solution is widely used in post-combustion due to its high reactivity and efficiency with fast kinetics and a strong chemical reaction, greater suitability, ease of reuse and low absorption of hydrocarbon [4–9]. However, there are several drawbacks, including: a large absorber size; high energy consumption for solvent regeneration; degradation of amine by SO_2, NO_2 and O_2 in the flue gases; and a high equipment-corrosion rate, leading to high operating costs [10–13].

Adsorption using solid adsorbents is one of the potential alternative methods that have been proposed to overcome the absorption disadvantages in term of cost for sorbent regeneration and corrosion problems [14]. It can also be operated over a wide range of temperatures and pressures [15]. Potential solid adsorbents for CO_2 adsorption should possess low heat capacity for easy regeneration, high stability and high surface contact between the adsorbent and CO_2, for example, zeolite (5A and 13X) [16], activated carbon [17–20], mesoporous silica (SBA-12, SBA-15, MCM-41, and KIT-6) [21–24], multiwalled-carbon nanotube [25], silica gel [26] and metal organic framework [27–29], etc. To increase the selectivity and the adsorption efficiency, the surface of the adsorbent is modified with an active functional group by either impregnation or grafting, such as monoethanolamine (MEA), diethanolamine (DEA), ethylenediamine (EDA), diethylenetriamine (DETA), triethylenetetramine (TETA), polyethyleneimine (PEI), 3-aminopropyl ethoxysilane (APES), 3-(methylamino)propyl ethoxysilane (MAPES), 3-aminopropyltriethoxysilane (APTES) and gaseous ammonia, etc. [25, 30–35]. Amine active sites attached on the surface of the porous adsorbent can react with CO_2 by a chemical reaction via the formation of carbamate and carbonate, which is a similar pathway to the CO_2-absorption mechanism [36–38]. The reaction pathways can be the carbamate formation (Equation (1)) followed by hydrolysis of carbamate to form bicarbonate (Equation (2)) or the hydrolysis of CO_2 to form bicarbonate (Equation (3)). The reactions of primary and secondary amines follow Equations (1) and (2), while tertiary amine follows Equation 3 through a base-catalysis mechanism:

$$CO_2 + 2RNH_2 \leftrightarrow RNHCOO^- + RNH_3^+ \quad (1)$$

$$RNHCOO^- + H_2O \leftrightarrow RNH_2 + HCO_3^- \quad (2)$$

$$CO_2 + R_3N + H_2O \leftrightarrow R_3NH^+ + HCO_3^- \quad (3)$$

Mesoporous silica is one of the most interesting adsorbents for CO_2 capture due to a high surface area with a high pore volume and also varieties of porous structures that

can be modified with amines by both impregnation and grafting onto the mesoporous silica. There are many literature studies about the CO_2-adsorption performance of amine-modified mesoporous silica. In 2013, Kamarudin and Alias synthesized MCM-41 and modified with MEA and DEA via the impregnation method to investigate the CO_2-adsorption performance. It was found that the adsorption capacity of MCM-41 modified with MEA and DEA was higher than that of pure MCM-41. In addition, the adsorption capacity was also increased with increasing amine loading [23]. Li et al. prepared SBA-15 via ethanol extraction and grafted with different kinds of (mono-, di- and tri-) aminosilanes. The CO_2 adsorption of unmodified and modified SBA-15 was tested at 25°C using 10% CO_2 (in N_2 balance) as a feed gas. It was found that the CO_2-adsorption capacity was increased from 0.21 to 1.07, 0.99 and 1.19 mmol/g for 3-aminopropyltrimethoxysilane-, *N*-[3-(trimethoxysilyl)propyl] ethylenediamine- and (3-trimethoxysilylpropyl)diethylenetriamine-modified SBA-15, respectively. The adsorption capacity increased with the increasing number of active amine sites in the structure [39]. In 2015, Kishor and Ghoshal studied the CO_2-adsorption performance of KIT-6 grafted with APTES. KIT-6 with 1.43, 1.50 and 1.72 mmol/g of APTES loading showed a CO_2-adsorption capacity of 0.76, 0.90 and 0.83 mmol/g, respectively. The result indicated that the adsorption capacity depended on the amine loading. The adsorbents also showed stable performance after 10 cycles of use [40]. Ullah et al. synthesized SBA-15 mesoporous silica and impregnated with hydroxylamine (NH_2OH). They reported that the CO_2 uptake of unmodified and modified SBA-15 at 25°C and 1 bar were 0.64 and 1.65 mmol/g, respectively [21]. In 2017, Hori et al. synthesized MCM-41, SBA-15 and KIT-6. They were modified with APTES, (3-aminopropyl) dimethyl ethoxysilane (APDMS), and (N-butylaminopropyl) trimethoxysilane (BAPS) to study the effect of pore size, aminosilane density and aminosilane molecular length on the CO_2-adsorption performance. They found that modified mesoporous silica with a smaller pore size, such as MCM-41 and SBA-15, showed a lower CO_2-adsorption capacity at high aminosilane density, while SBA-15 with expanded pores and KIT-6 with larger pore size were better in both adsorption capacity and kinetics [41].

From the literature, the different porous characteristics of an adsorbent have a high impact on its kinetics and efficiency for CO_2 capture. In addition, based on the literature, most CO_2-adsorption research has studied and investigated the important performances of CO_2-adsorption capacity, cyclical use and also kinetics. However, some other equally important performances such as the heat duty for adsorbent regeneration need to be considered to fulfil the best criteria for selecting the adsorbent for CO_2 capture. In CO_2-absorption technology, the energy requirement for solvent regeneration covers 70% of the operating cost. A good adsorbent/absorbent should show great performance in both adsorption and desorption with a low energy requirement for regeneration. Then, the energy requirement of the adsorbent is one of the parameters that need to be emphasized. Yamada et al. studied the CO_2 adsorption/desorption efficiency of tetraethylenepentamine (TEPA)-modified silica and also investigated the energy consumption for regeneration. The estimated heat duty was 1.5 GJ/ton CO_2 for a steam-aided vacuum-swing adsorption process [42]. Gray et al. also estimated the heat duty for the regeneration of amine-based solid adsorbent. It was 1.2–2.3 GJ/ton CO_2 [43]. Plaza et al. used a carbon honeycomb monolith as an adsorbent for CO_2 capture. The heat duty for adsorbent regeneration in a temperature-swing adsorption (TSA) process was investigated to be 3.59 MJ/kg CO_2 [44].

In this work, mesoporous silicas with different morphologies such as MCM-41, SBA-15 and KIT-6 were synthesized and the surface modified with APTES to investigate the effect of a porous structure of adsorbents on CO_2-adsorption activities including adsorption capacity, adsorption rate, desorption characteristic, regeneration efficiency, heat duty for adsorbent regeneration and also cyclic use.

1 Experimental

1.1 Materials and methods

Tri-block copolymer pluronic P123 surfactant with molecular weight ~5800, tetraethyl orthosilicate (TEOS, 98%), ammonia solution (30%), APTES (99%) and cetyltrimethylammonium bromide (CTAB, ≥98%) were purchased from Sigma Aldrich. Anhydrous toluene (AR grade), n-butanol (AR grade), methanol (AR grade) and fuming hydrochloric acid (HCl, 37%) were purchased from RCI Labscan, Thailand. GC-grade nitrogen (N_2, 99.99%) and premixed gas containing 15 vol% CO_2 with N_2 balance were obtained from Praxair.

1.2 Synthesis of MCM-41, SBA-15 and KIT-6 mesoporous silica

MCM-41 was synthesized using the procedure described in the previous work reported by Loganathan et al. [45]. Typically, it was synthesized by dissolving 2 g of CTAB in 120 mL of deionized water and stirring for 30 mins. Then, 7.5 mL of 30 wt% ammonia solution was added and stirred for 1 hr. Then, 10 mL of TEOS was further added into the mixture solution and stirred at room temperature for 12 hrs. The sample solution was filtered and washed with distilled water until neutral and dried at 100°C for 12 hrs. The sample powder was ground before calcination at 550°C with a heating rate of 10°C/min for 5 hrs.

SBA-15 was synthesized using the procedure described in the previous work reported by Yan et al. [46]. Four grams of Pluronic P123 were dissolved in 144 mL of 1.7 M HCl solution and the mixture was completely dissolved at 40°C.

Then, 9.2 mL of TEOS was added into the mixture solution and further stirred at 40°C for 24 hrs. The mixture was transferred into a Teflon-lined autoclave and aged at 100°C for 24 hrs. The suspension sample was filtered, washed with distilled water until neutral and dried at 100°C for 24 hrs. The obtained white powder was ground prior to calcination at 550°C with a heating rate of 10°C/min for 24 hrs.

The procedure for synthesizing KIT-6 was described by Kishor and Ghoshal [47]. Four grams of Pluronic P123 were dissolved in 150 mL of 0.5 M HCl solution and stirred at 40°C for 1 hr. Then, 4.94 mL of n-butanol was added into the solution and stirred for 1 hr; 9.15 mL of TEOS was added and stirred at 40°C for 24 hrs. The sample solution was transferred to a Teflon-lined autoclave and aged at 100°C for 24 hrs. The sample was filtered, washed with distilled water until neutral and then dried at 100°C for 24 hrs. The white-powder sample was ground prior to calcination at 550°C with a heating rate of 10°C/min for 5 hrs.

1.3 Grafting of APTES on mesoporous silicas

First, 10 mL of APTES was dissolved in 50 mL of anhydrous toluene. Then, 1 g of synthesized mesoporous silica was added to the solution. The reaction was stirred and refluxed at 120°C for 24 hrs. The sample suspension was filtered and washed with toluene and methanol, then dried at 80°C for 24 hrs. This procedure was previously reported by Fijjiki et al. [48].

1.4 Characterization

The morphology of MCM-41, SBA-15 and KIT-6 was studied using a Hitachi S-4800 Field Emission Scanning Electron Microscope (FE-SEM) and JEM-1400 Transmission Electron Microscope (TEM). For FE-SEM, the sample powder was pressed on an aluminium stub with conductive carbon tape and coated with platinum sputtering for about 5 mins.

X-ray diffraction (XRD) measurement was performed using a Rigaku powder diffractometer (Rigaku, Japan) with CU Kα radiation. The tube voltage was 40 kV and the current was 40 mA. The XRD patterns were taken in the 2θ range of 0.5–10° at a scan speed of 0.5°/min to investigate the crystal pattern of the obtained mesoporous silicas.

The surface area, pore volume and pore size of the mesoporous silica were measured by N_2 adsorption/desorption on a Quantachrome Autosorp1-MP. Mesoporous silica and modified mesoporous silica powder samples were degassed at 250°C under N_2 flow for 24 hrs prior to analysis. The surface area was calculated using the Brunauer–Emmett–Teller equation. The pore-size distribution was determined using the Barette–Joyner–Halenda method. The total pore volume was calculated from the amount of adsorbed N_2 at $P/P_0 = 0.99$.

The reaction between the APTES and mesoporous silica was monitored using a Fourier transform infrared spectrophotometer (FTIR, model Nexus 670, Bruker).

The amount of amine loaded onto the modified mesoporous silica was determined using a thermal gravimetric analyser (TGA, Mettler Toledo). The sample powder was heated at a heating rate of 10°C/min in N_2 atmosphere with a flow rate of 15 mL/min.

1.5 CO_2 adsorption/desorption test

First, 0.5 g of adsorbent was packed in a stainless-steel reactor, pretreated by allowing N_2 to flow through the adsorbent with a flow rate of 20 mL/min at 100°C for 1 hr to remove residual gases or moisture trapped inside the adsorbent and then cooled to room temperature. The adsorption test was performed at room temperature and atmospheric pressure. After the pretreatment step was completed, the N_2 gas was then switched to 15% CO_2 in N_2 balance with a flow rate of 20 mL/min. The CO_2 feed gas was allowed to purge into the reactor and the CO_2 concentration at the outlet was continuously detected using a gas chromatograph equipped with a thermal-conductivity detector (GC-TCD; Agilent, model 7280A) fitted with a Porapak-Q column (0.32 mm id × 60 m *l* dimension) until saturation (the CO_2 concentration in effluent gas equals the feed concentration). When the CO_2 adsorption was completed, the desorption experiment was subsequently carried out by switching the CO_2 feed gas to the N_2 gas at a flow rate of 20 mL/min together with applying heat at 100°C using heating tape. The desorption experiment was carried out by continuously detecting the CO_2 concentration until there was no CO_2 peak found in the chromatogram. The experimental set-up for the CO_2 adsorption/desorption is shown in Fig. 1.

The dynamic adsorption capacity (Q_{ads}) was determined by collecting the CO_2-concentration responses and plotting between C_{ou}/C_{in} and time as a breakthrough curve. The Q_{ads} of the adsorbent could be calculated using Equation (4) [49]:

$$Q_{ads} = \frac{FC_{in}t_{st}}{M} \quad (4)$$

where Q_{ads} is the dynamic adsorption capacity (molCO_2/g-adsorbent), *F* is the total flow rate (mol/min), C_{in} is the concentration of CO_2 entering the reactor (vol%), *M* is the

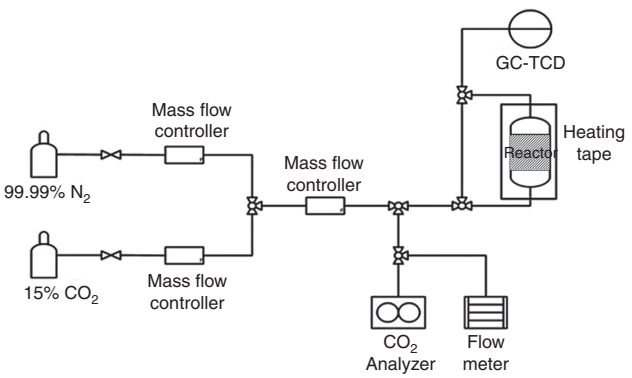

Fig. 1: Experimental set-up for CO_2 adsorption/desorption test

weight of the adsorbent (g) and t_{st} is the stoichiometric time corresponding to the CO_2 stoichiometric adsorption capacity (min). The stoichiometric adsorption capacity can be shown to be proportional to the area between the breakthrough curve and the line at $C_{ou}/C_{in} = 1.0$. The t_{st} can be calculated by using Equation (5) [49]:

$$t_{st} = \int_0^t \left(1 - \frac{C_{ou}}{C_{in}}\right) dt \quad (5)$$

where C_{ou} is the concentration of CO_2 downstream of the reactor (vol%) and t is the time at which the C_{ou} reaches its maximum level (min).

The CO_2-adsorption rate of the adsorbent was determined at three stages including the early, middle and final stages, which could be determined from the linear portion from the slope of the plot between the Q_{ads} and the time at different stages. The CO_2 adsorption at time intervals was also calculated using Equations (1) and (2). The desorption efficiency of the adsorbents represents the regenerability of the adsorbent after CO_2 was removed from the first run, which could be calculated from the Q_{ads} of the first adsorption and the second adsorption. The heat duty for the adsorbent regeneration (Q_{reg}, kJ/mmolCO_2) was calculated based on Equations (6) and (7) adopted from Singto et al. [50]:

$$Q_{reg} = \frac{q}{CO_2\ produced} \quad (6)$$

$$q = \frac{KAdt}{dx} \quad (7)$$

where q is the heat transfer (W); the CO_2 produced (mmolCO_2/g.s) is obtained from the CO_2-adsorption capacity of the second run of CO_2 adsorption; K is the thermal conductivity of the stainless-steel reactor (16.5 W/mK); A is the surface area of the cylindrical sector of the adsorbent in the reactor (m^2); dt is the temperature difference between the inside and the outside of the reactor (K) and dx is the thickness of the reactor (m).

2 Results and discussion

2.1 Morphology and surface properties of amine-modified mesoporous silica

The XRD patterns of MCM-41, SBA-15 and KIT-6 are shown in Fig. 2. A hexagonal close-packed structure of MCM-41 and SBA-15 showed a peak at 2θ of 2.6° (d_{100}) and 0.90° (d_{100}), respectively. A gyroidal cubic la3d structure of KIT-6 showed a peak at 2θ of 0.95° (d_{211}) [47, 51–53]. From the SEM and TEM micrographs of the synthesized mesoporous silica (Fig. 3), MCM-41 and SBA-15 showed a 2D hexagonal structure with parallel cylindrical pore channels in which the pore size of SBA-15 was larger than that of MCM-41. The particle sizes of MCM-41 and SBA-15 were 0.3 × 0.8 and 0.5 × 1.8 μm, respectively. KIT-6 showed well-ordered and interconnected pore channels with a particle size of 2.6 μm. These results

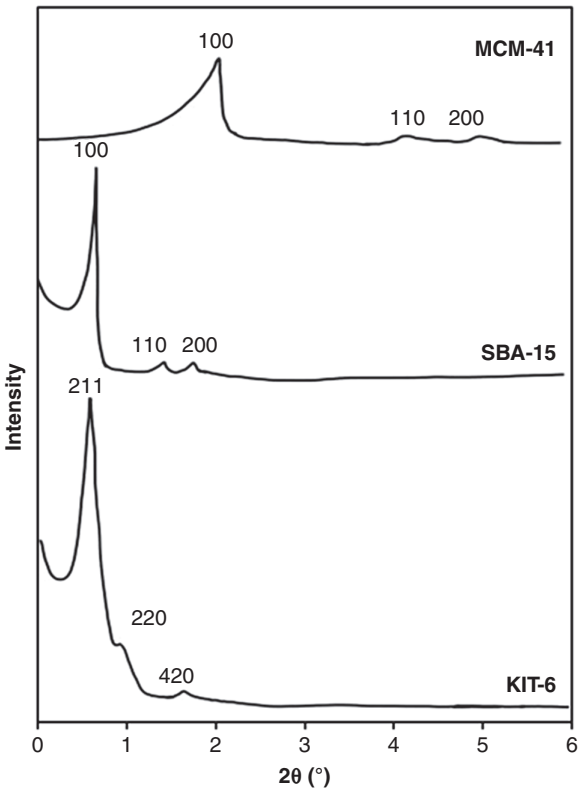

Fig. 2: XRD patterns of MCM-41, SBA-15 and KIT-6

could confirm the formation of a synthesized mesoporous silica that had similar morphology to that reported in the literature [52, 54]. The typical structure data of MCM-41, SBA-15 and KIT-6 are shown in Table 1. MCM-41 showed the highest surface area of 1007 m^2/g with 0.944 cm^3/g of pore volume and 2.91 nm of pore size. SBA-15 showed a surface area of 737 m^2/g with 1.23 cm^3/g of pore volume and 6.15 nm of pore size, while KIT-6 showed the lowest surface area of 672 m^2/g with 0.99 cm^3/g of pore volume and 8.02 nm of pore size.

APTES can be employed to modify mesoporous silica via grafting with the reaction between the silanol group of APTES and the OH group on mesoporous silica, which was confirmed by the FTIR spectra (Fig. 4). A broad band of ~3500–3100 cm^{-1} on unmodified mesoporous silicas is attributed to the OH stretching vibration of silanol groups (SiOH) and absorbed moisture [55]. The asymmetric and symmetric stretching vibrations of Si–O–Si were observed at ~1070 and 790 cm^{-1}, respectively. After modification, the decrease in the FTIR absorption of the SiOH group was observed together with the presence of the asymmetric and symmetric stretching vibrations of CH_2 in the propyl group at 2926 and 2848 cm^{-1}, respectively. Stretching vibration of C–C and C–N also showed at a wave numbers of 1571 and 1479 cm^{-1} [56].

The amount of APTES loaded onto mesoporous silicas was determined by observing the weight loss in the TGA profile. Fig. 5 shows the TGA profiles of the APTES_MCM-41, APTES_SBA-15 and APTES_KIT-6 adsorbents during

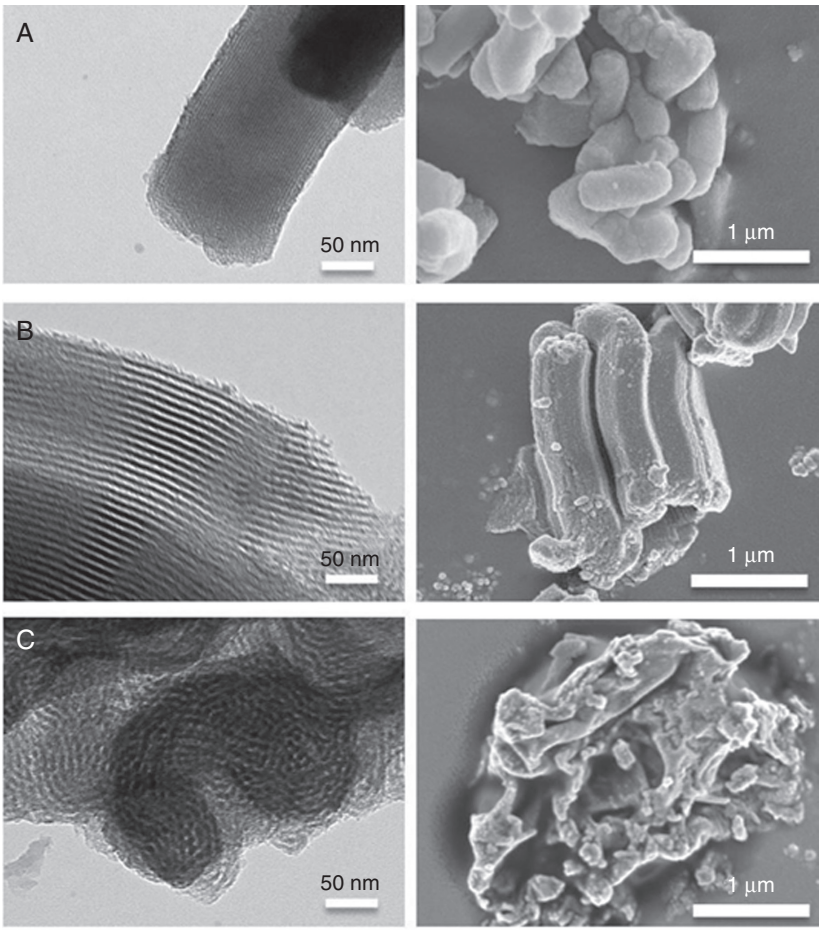

Fig. 3: TEM and SEM micrographs of (a) MCM-41, (b) SBA-15 and (c) KIT-6

Table 1: Surface properties, amine loading, adsorption capacity (Q_{ads}) and heat duty for the adsorbent regeneration (Q_{ads}) of unmodified and modified mesoporous silicas

Adsorbents	Surface area (m^2/g)	Pore size (nm)	Pore volume (cc/g)	Amine loading (mmol/g)	Q_{ads} ($mmolCO_2/g$)	Q_{reg}($kJ/mmolCO_2$)
MCM-41	1007	2.91	0.94	–	0.63	21.66
SBA-15	737	6.15	1.24	–	0.71	3.72
KIT-6	672	8.02	0.99	–	0.52	2.55
APTES_MCM-41	58.1	1.78	0.12	1.82	1.01	26.50
APTES_SBA-15	20.1	6.05	0.13	3.04	1.75	20.45
APTES_KIT-6	16.2	6.1	0.09	1.64	1.30	12.07

heating in N_2 atmosphere. The weight loss between room temperature and 200°C corresponds to the release of adsorbed moisture. The observed weight loss in the temperature range of 200–700°C represents the degradation of the 3-aminopropyl site. The weight loss observed in the temperature range of 200–700°C was 10.56% for APTES_MCM-41, 17.63% for APTES_SBA-15 and 9.51% for APTES_KIT-6, which correspond to 1.82, 3.04 and 1.64 mmol of aminopropyl (or $–NH_2$-adsorption sites) per gram of silica, respectively (see Table 1). After APTES modification, the surface area, pore volume and pore diameter of the synthesized mesoporous silica were significantly reduced, as seen in Table 1. The pore volume of MCM-41, SBA-15 and KIT-6 was reduced to 0.12, 0.13 and 0.09 cm^3/g, respectively. The surface areas were consequently reduced to 58.1, 20.1 and 61.2 m^2/g, respectively. The reduction in the pore diameter was in the order of APTES_MCM-41 (1.78 nm) < APTES_SBA-15 (6.05 nm) < APTES_KIT-6 (6.10 nm). This reduction was caused by pore blockage by the amino groups in the adsorbent. These results were also observed in the previous work on the modification of mesoporous silica with amine [57].

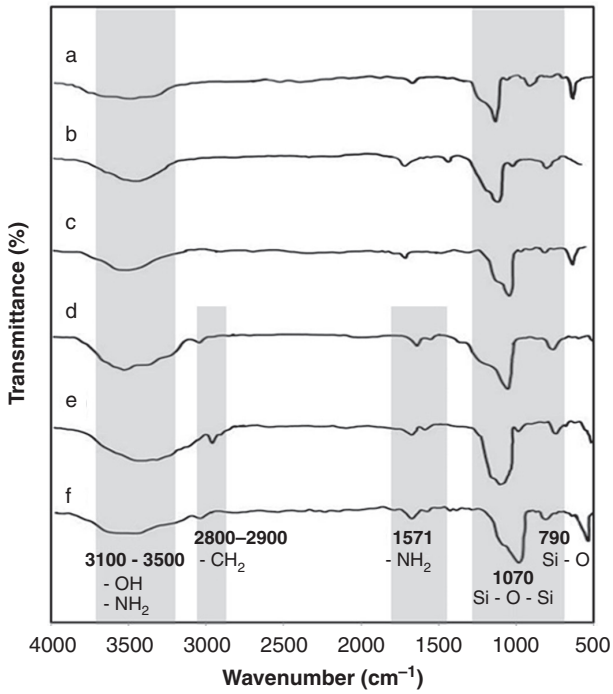

Fig. 4: FTIR spectra of adsorbents. (a) MCM-41; (b) SBA-15; (c) KIT-6; (d) APTES_MCM-41; (e) APTES_SBA-15; and (f) APTES_KIT-6.

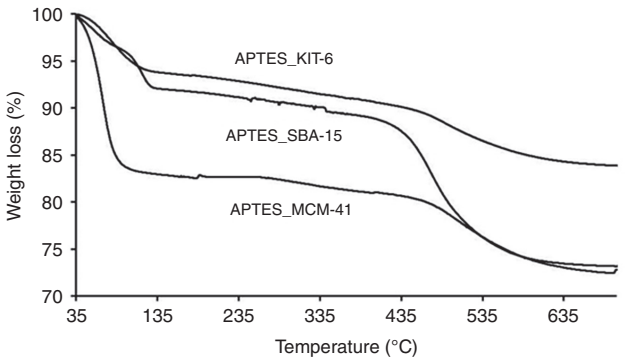

Fig. 5: TGA profiles of the APTES_MCM-41, APTES_SBA-15 and APTES_KIT-6

2.2 CO_2-adsorption capacity and CO_2-adsorption rate

Adsorption experiments were carried out at room temperature and atmospheric pressure using 15% CO_2 (in N_2 balance) with a flow rate of 20 mL/min. The adsorption capacity was calculated based on the breakthrough profile using Equations (4) and (5). The CO_2 uptake at the saturation point is called the dynamic adsorption capacity (Q_{ads}). All unmodified adsorbents reached the breakthrough point in <1 min with Q_{ads} of 0.63, 0.71 and 0.52 mmolCO_2/g-adsorbent for MCM-41, SBA-15 and KIT-6, respectively. MCM-41 with the highest surface area (1007 m^2/g) did not show the highest Q_{ads} due to the smallest pore-size diameter and micropore volume, which could obstruct the transportation of CO_2 molecules along the adsorbent at atmospheric pressure. SBA-15 (surface area = 732 m^2/g) with the largest pore-size diameter (6.15 nm) showed the highest Q_{ads} among the unmodified adsorbents. KIT-6 with the lowest surface area and the largest pore diameter showed the lowest Q_{ads}. From the results, it was indicated that a high surface area is not the only important factor influencing adsorption capacity; the pore-size diameter must also be considered. For the kinetics of adsorption, the adsorption rate was investigated by inspecting the linear portion of the adsorption profile (see Fig. 6) in different ranges of adsorption times. At the early stage, the slope of the adsorption profile was sharper than those of the middle and the final stages, which meant that the highest adsorption rate was obtained at the early stage. The adsorption rate decreased at the middle and the final stages. The limitation of the pore diameter of MCM-41 also affected the CO_2-adsorption rate. At the early stage of adsorption, the CO_2 was adsorbed onto MCM-41 with an adsorption rate of 9.55×10^{-2} mmolCO_2/g.min. The adsorption at the early stage was contributed by the mesopore channel, which provided good mass transfer. At the middle and final stages, the adsorption rates decreased to 0.91×10^{-2} and 0.45×10^{-2} mmolCO_2/g.min because the CO_2 molecules were transported in the microchannels that had high mass-transfer resistance. The adsorption rates of SBA-15 and KIT-6 were quite similar due to the main existence of mesopore channels. The adsorption rates at all stages of all adsorbents are shown in Fig. 7. SBA-15 showed adsorption rates at the early, middle and final stages of 13.09×10^{-2}, 0.56×10^{-2} and 0.36×10^{-2} mmolCO_2/g.min, respectively. KIT-6 showed adsorption rates at the early, middle and final stages of 12.78×10^{-2}, 0.51×10^{-2} and 0.57×10^{-2} mmolCO_2/g.min, respectively. Mesopore channels provide better transfer of CO_2 in the adsorbent. In addition, the interconnected pore structure of KIT-6 also provided better mass transfer of CO_2 throughout the adsorbent than that of SBA-15 as obviously seen in the final stage of adsorption [58].

After modification with APTES, the CO_2 breakthrough point of all modified adsorbents was delayed. The Q_{ads} of APTES_MCM-41, APTES_SBA-15 and APTES_KIT-6 increased to 1.01, 1.75 and 1.30 mmolCO_2/g-adsorbent, respectively. The Q_{ads} of the modified adsorbent was enhanced due to the presence of the primary amine that promoted the chemical adsorption by forming carbamate via the Zwitterion mechanism with one molecule of CO_2 reacting with two amine sites to form the carbamate in dry conditions. APTES_SBA-15 showed the highest Q_{ads} due to the highest amine loading of 3.04 mmol/g, while APTES_MCM-41 and APTES_KIT-6 with amine loading of 1.82 and 1.64 mmol/g showed lower adsorption capacity. From these results, it was suggested that the amount of amine loading played an important role for CO_2 adsorption according to chemical adsorption. The adsorption rates of all modified adsorbents increased to 11.2×10^{-2}, 13.76×10^{-2} and 16.7×10^{-2} mmolCO_2/g.min for the early stages of

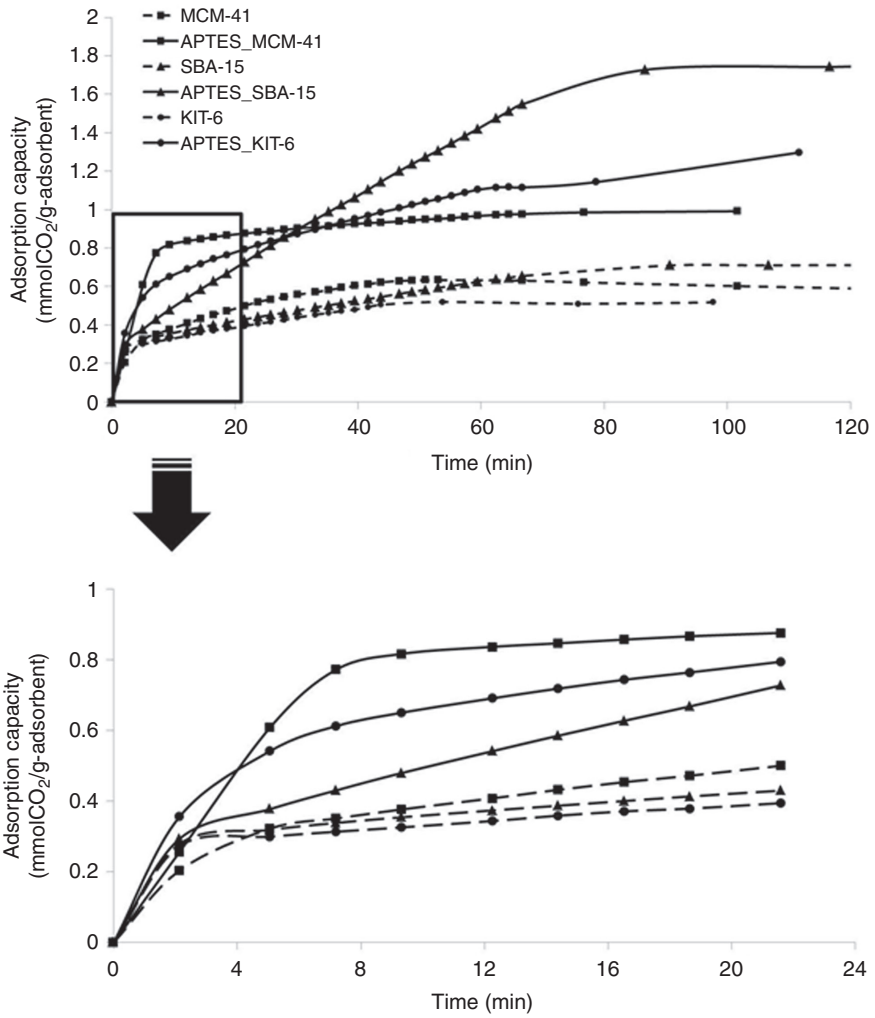

Fig. 6: Adsorption profile of unmodified and modified mesoporous silicas

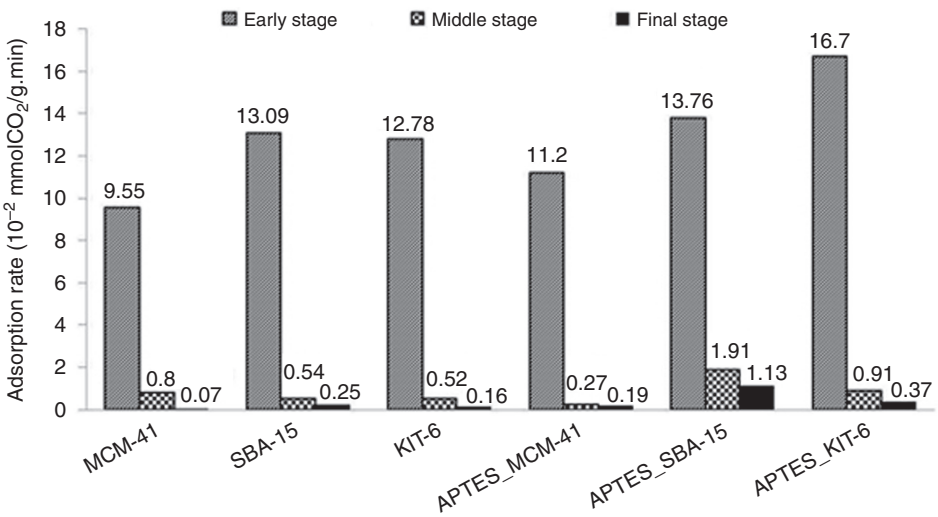

Fig. 7: The CO_2-adsorption rate at early, middle and final stages of all adsorbents

APTES_MCM-41, APTES_SBA-15 and APTES-KIT-6, respectively. This was due to the fast reaction between CO_2 and the primary amine together with the transport of the CO_2 in the mesopore channels. In the middle and final stages, the adsorption rate decreased due to the transportation of the CO_2 molecules in the smaller pore channels. From the results,

it can be concluded that mesoporous silica with a larger pore size, high pore volume and also 3D interconnected structure could gain the benefit of amine loading—an easy pathway for CO_2 molecules to achieve the greater adsorption capacity and also adsorption kinetics [46, 59–62].

2.3 Heat duty (Q_{reg}) and regenerability of adsorbents

All unmodified adsorbents could rapidly release CO_2 at 100°C because of the weak interaction between the CO_2 and the adsorbent surface via physical interaction. MCM-41 containing micropore channels took around 8 mins for releasing CO_2 so more energy was required for the regeneration (21.66 kJ/mmolCO_2). SBA-15 and KIT-6 took around 3 mins to release the CO_2 with Q_{reg} of 3.72 and 2.55 kJ/mmolCO_2. KIT-6, with a cubical interconnected large pore diameter, provides good transportation of the N_2 flow for purging the CO_2 out, resulting in the lowest Q_{reg}. In the case of APTES-modified adsorbents, APTES_SBA-15 took around 69 mins to release CO_2 at 100°C with Q_{reg} of 20.45 kJ/mmolCO_2. The higher primary amine loading in SBA-15 formed larger amounts of stable carbamate during the adsorption process, resulting in the higher energy requirement for regeneration. APTES_MCM-41 required 26.50 kJ/mmolCO_2 to release the CO_2. Even though it contained lower amine loading than APTES_SBA-15, it required higher energy. This was due to the smaller size of the channels through which the gas could travel, so it took more time to remove the CO_2 out of the adsorbent, resulting in the highest energy requirement. The advantages of the larger pore size and interconnected porous structure in KIT-6 gave good CO_2-desorption performance, leading to the lowest energy requirement for the regeneration of APTES_KIT-6 (12.07 kJ/mmolCO_2). When comparing the Q_{ads} of cycle 1 and cycle 2 (see Table 1) to determine the efficiency of adsorbent regeneration, it was found that the regeneration efficiency at 100°C of unmodified and modified adsorbents reached 95%.

For practical application, a good adsorbent should show a good regenerability of the cyclic adsorption/desorption process for long-term operation. In this study, five cycles of the adsorption/desorption of APTES-modified adsorbents were performed. The breakthrough profiles of five adsorption/desorption cycles of each modified adsorbent are shown in Fig. 8. The Q_{ads} of each adsorbent after each cycle is shown in Fig. 9. After five cycles, the Q_{ads} was decreased from 1.01 to 0.95 mmolCO_2/g-adsorbent for APTES_MCM-41, from 1.75 to 1.55 mmolCO_2/g-adsorbent for APTES_SBA-15 and from 1.30 to 1.11 mmolCO_2/g-adsorbent for APTES_KIT-6. The stability of the amine-modified adsorbent was related to the stability of the amine sites after many adsorption/desorption cycles. The porous structure of the adsorbent does not play an important role in this point. The decrease in Q_{ads} could be because of the strong bond between the CO_2 and the primary amine in APTES, resulting in the incomplete desorption of pre-adsorbed CO_2 at 100°C. This result was also reported in previous work [56, 63].

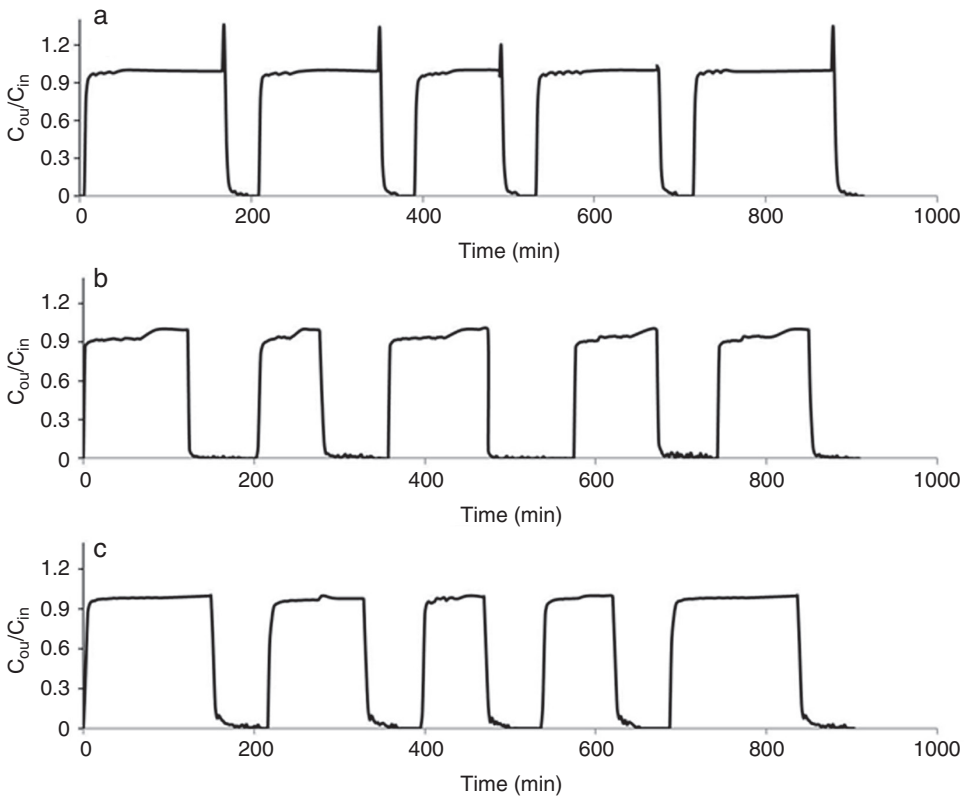

Fig. 8: Breakthrough profiles of CO_2 adsorption/desorption cycles of APTES_MCM-41 (a), APTES_SBA-15 (b) and APTES_KIT-6 (c)

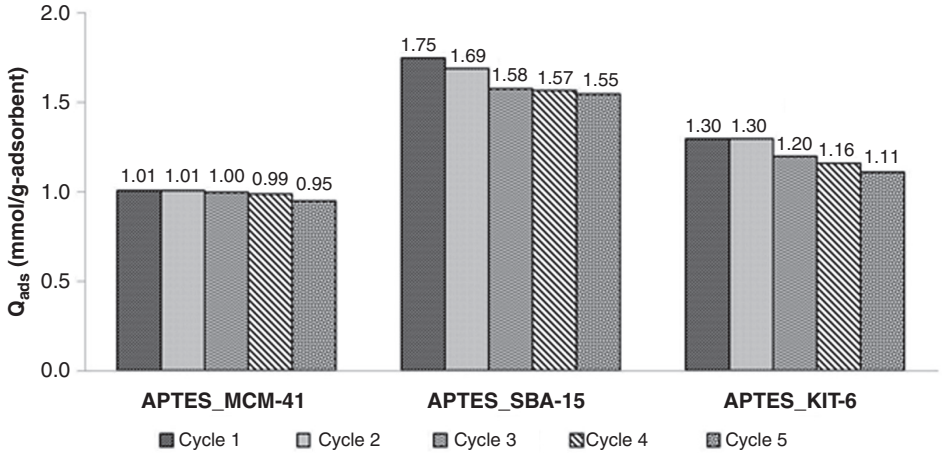

Fig. 9: Cyclic adsorption/desorption performance of APTES_MCM-41, APTES_SBA-15 and APTES_KIT-6. Adsorption temperature: room temperature; 15% CO_2 gas flow rate: 15 mL/min; desorption temperature: 100°C; N_2 flow rate: 20 mL/min).

3 Conclusions

In this study, mesoporous silicas with different textural porous structures such as MCM-41, SBA-15 and KIT-6 were synthesized and functionalized with APTES to improve the selectivity for CO_2. The maximum amine loading was achieved in SBA-15 due to a large-enough pore size and pore volume. The CO_2-adsorption capacity depended on the number of amine sites and also the pore-size diameter of the adsorbents. In addition, the pore-size diameter and also pore structure of the adsorbent also affected the kinetics of the CO_2 adsorption; a larger pore size with an interconnected porous structure provided a good pathway for CO_2 molecules towards active amine sites in the adsorption process and also for N_2 purging and heat transfer during the desorption process. Hence, a promising adsorbent should possess a moderate pore-size diameter with a high-enough surface area, pore volume and interconnected pore structure because this can maintain good properties for adsorption after modification and also promote the diffusion of gas throughout the adsorbent that can both increase the adsorption/desorption kinetics and require less energy for regeneration.

Acknowledgements

We gratefully acknowledge financial support from Ratchadaphiseksomphot Endowment Fund, Chulalongkorn University and the Sustainable Petroleum and Petrochemicals Research Unit under the Center of Excellence on the Petrochemical and Materials Technology, Chulalongkorn University.

Conflict of Interest

None declared.

References

[1] Song G, Zhu X, Chen R, et al. An investigation of CO_2 adsorption kinetics on porous magnesium oxide. *Chem Eng J* 2016; 283:175–83.
[2] Oh J, Mo YH, Le VD, et al. Borane-modified graphene-based materials as CO_2 adsorbents. *Carbon* 2014; 79:450–6.
[3] Fogarty D. *Global CO_2 emissions to hit record in 2018*, *The Straits Times*, 2018. https://www.straitstimes.com/world/global-carbon-dioxide-emissions-from-fossil-fuels-to-hit-record-this-year-says-study (12 March 2020, date last accessed).
[4] Yang H, Xu Z, Fan M, et al. Progress in carbon dioxide separation and capture: a review. *J Environ Sci* 2008; 20:14–27.
[5] Li L, Zhao N, Wei W, et al. A review of research progress on CO_2 capture, storage, and utilization in Chinese Academy of Sciences. *Fuel* 2013; 108:112–30.
[6] Cousins A, Wardhaugh LT, Feron PHM. A survey of process flow sheet modifications for energy efficient CO_2 capture from flue gases using chemical absorption. *Int J Greenh Gas Con* 2011; 5:605–19.
[7] Hammond GP, Spargo J. The prospects for coal-fired power plants with carbon capture and storage: a UK perspective. *Energy Convers Manag* 2014; 86:476–89.
[8] Sema T, Naami A, Liang Z, et al. Analysis of reaction kinetics of CO_2 absorption into a novel reactive 4-diethylamino-2-butanol solvent. *Chem Eng Sci* 2012; 81:251–9.
[9] Donaldson TL, Nguyen YN. Carbon dioxide reaction kinetics and transport in aqueous amine membranes. *Ind Eng Chem Fundam* 1980; 19:260–6.
[10] Ramachandran N, Aboudheir A, Idem R, et al. Kinetics of the absorption of CO_2 into mixed aqueous loaded solutions of monoethanolamine and methyldiethanolamine. *Ind Eng Chem Res* 2006;45:2608–16.
[11] Brunetti A, Scura F, Barbieri G, et al. Membrane technologies for CO_2 separation. *J Membr Sci* 2010; 359:15–125.
[12] Hook RJ. An investigation of some sterically hindered amines as potential carbon dioxide scrubbing compounds. *Ind Eng Chem Res* 1997; 36:1779–90.

[13] Hagewiesche DP, Ashour SS, Al-Ghawas HA, et al. Absorption of carbon dioxide into aqueous blends of monoethanolamine and N-methyldiethanolamine. *Chem Eng Sci* 1995; 50:1071–9.

[14] Tontiwachwuthikul P, Meisen A, Lim CJ. Solubility of carbon dioxide in 2-amino-2-methyl-1-propanol solutions. *J Chem Eng Data* 1991; 36:130–3.

[15] Duffy A, Walker GM, Allen SJ. Investigations on the adsorption of acidic gases using activated dolomite. *Chem Eng J* 2016; 117:239–44.

[16] Garces-Polo SI, Villarroel-Rocha J, Sapag K, et al. A comparative study of CO_2 diffusion from adsorption kinetic measurements on microporous material at low pressures and temperatures. *Chem Eng J* 2016; 302:278–86.

[17] Rashidi NA, Yusup S, Lam HL. Kinetic studies on carbon dioxide capture using activated carbon. *Chem Eng Trans* 2013; 35:361–6.

[18] Guo B, Chang L, Xie K. Adsorption of carbon dioxide on activated carbon. *J Nat Gas Chem* 2006; 15:223–9.

[19] Dantas TLP, Luna FMT, Silva IJ, et al. Carbon dioxide–nitrogen separation through adsorption on activated carbon in a fixed bed. *Chem Eng J* 2011; 169:11–9.

[20] Shafeeyan MS, Daud WMAW, Houshmand A, et al. A review on surface modification of activated carbon for carbon dioxide adsorption. *J Anal Appl Pyrolysis* 2010; 89:143–51.

[21] Ullah R, Atillhan M, Aparicio S, et al. Insights of CO_2 adsorption performance of amine impregnatedmesoporous silica (SBA-15) at wide range pressure and temperature conditions. *Int J Greenh Gas Con* 2015; 43:22–32.

[22] Liu Y, Shi J, Chen J, et al. Dynamic performance of CO_2 adsorption with tetraethylenepentamine-load KIT-6. *Microporous Mesoporous Mater* 2010; 134:16–21.

[23] Kamarudin KSN, Alias N. Adsorption performance of MCM-41 impregnated with amine for CO_2 removal. *Fuel Process Technol* 2013; 106:332–7.

[24] Chang ACC, Chuang SSC, Gray M, et al. In-situ infrared study of CO_2 adsorption on SBA-15 grafted with γ-(aminopropyl) triethoxysilane. *Energy Fuels* 2003; 16:468–73.

[25] Hsu SC, Lu C, Su F, et al. Thermodynamics and regeneration studies of CO_2 adsorption on multiwalled carbon nanotubes. *Chem Eng Sci* 2010; 65:1354–61.

[26] Wang K, Shang H, Li L, et al. Efficient CO_2 capture on low-cost silica gel modified by polyethyleneimine. *J Nat Gas Chem* 2010; 21:319–23.

[27] Dietzel PDC, Besikiotis V, Blom R. Application of metal–organic frameworks with coordinatively unsaturated metal sites in storage and separation of methane and carbon dioxide. *J Mater Chem* 2009; 19:7362–70.

[28] Li JR, Ma Y, McCarthy MC, et al. Carbon dioxide capture-related gas adsorption and separation in metal–organic frameworks. *Coord Chem Rev* 2011; 255:1791–823.

[29] Sumida K, Rogow DL, Mason JA, et al. Carbon dioxide capture in metal-organic frameworks. *Chem Rev* 2012; 112:724–81.

[30] Chatti R, Bansiwal AK, Thote JA, et al. Amine loaded zeolites for carbon dioxide capture: amine loading and adsorption studies. *Microporous Mesoporous Mater* 2009; 121:84–9.

[31] Plaza MG, Pevida C, Arenillas A, et al. CO_2 capture by adsorption with nitrogen enriched carbons. *Fuel* 2007; 86:2204–12.

[32] Seko N, Bang LT, Tamada M. Syntheses of amine-type adsorbents with emulsion graft polymerization of glycidyl methacrylate. *Nucl Instrum Methods Phys Res Sect B* 2007; 265:146–9.

[33] Zelenak V, Halamova D, Gaberova L, et al. Amine-modified SBA-12 mesoporous silica for carbon dioxide capture: effect of amine basicity on sorption properties. *Microporous Mesoporous Mater* 2008; 116:358–64.

[34] Serna-Guerrero R, Sayari A. Modeling adsorption of CO_2 on amine-functionalized mesoporous silica. 2: Kinetics and breakthrough curves. *Chem Eng J* 2010; 161:182–90.

[35] Sayari A, Belmabkhout Y. Stabilization of amine-containing CO_2 adsorbents: dramatic effect of water vapor. *J Am Chem Soc* 2010; 132:6312–4.

[36] Rinker E, Ashour SS, Sandall OC. Absorption of carbon dioxide into aqueous blends of diethanolamine and methyldiethanolamine. *Ind Eng Chem Res* 2000; 39:4346–56.

[37] Hiyoshi N, Yogo K, Yashima T. Adsorption of carbon dioxide on amine modified SBA-15 in the presence of water vapor. *Chem Lett* 2014; 33:510–1.

[38] Dankwerts PV. The reaction of CO_2 with ethanolamines. *Chem Eng Sci* 1979; 34:443–5.

[39] Li Y, Sun N, Li L, et al. Grafting of amines on ethanol-extracted SBA-15 for CO_2 adsorption. *Material* 2013; 6:981–99.

[40] Kishor R, Ghoshal AK. APTES grafted ordered mesoporous silica KIT-6 for CO_2 adsorption. *Chem Eng J* 2015; 262:882–90.

[41] Hori K, Higuchi T, Aoki Y, et al. Effect of pore size, aminosilane density and aminosilane molecular length on CO_2 adsorption performance in aminosilane modified mesoporous silica. *Microporous Mesoporous Mater* 2017; 246:158–65.

[42] Yamada H, Chowdhury FA, Fujiki J, et al. Enhancement mechanism of the CO_2 adsorption-desorption efficiency of silica-supported tetraethylenepentamine by chemical modification of amino groups. ACS *Sustainable Chem Eng* 2019; 7:9574–81.

[43] Gray ML, Hoffman JS, Hreha DC, et al. Parametric study of solid amine sorbents for the capture of carbon dioxide. *Energy Fuels* 2009; 23:4840–4.

[44] Plaza MG, Rubiera F, Pevida C. Evaluating the feasibility of a TSA process based on steam stripping in combustion with structured carbon adsorbents to capture CO_2 from a coal power plant. *Energy Fuels* 2017; 31:9760–75.

[45] Loganathan S, Tikmani M, Ghoshal AK. Novel pore-expanded MCM-41 for CO_2 capture: synthesis and characterization. *Langmuir* 2013; 29:3491–9.

[46] Yan X, Zhang L, Zhang Y, et al. Amine-modified SBA-15: effect of pore structure on the performance for CO_2 capture. *Ind Eng Chem Res* 2011; 50:3220–6.

[47] Kishor R, Ghoshal AK. Understanding the hydrothermal, thermal, mechanical and hydrolytic stability of mesoporous KIT-6: a comprehensive study. *Microporous Mesoporous Mater* 2017; 242:127–35.

[48] Fujiki J, Yamada H, Yogo K. Enhanced adsorption of carbon dioxide on surface-modified mesoporous silica-supported tetraethylenepentamine: role of surface chemical structure. *Microporous Mesoporous Mater* 2015; 215:76–83.

[49] Geankoplis CJ. *Transport Processes and Unit Operations*, 4th edn. Upper Saddle River, NJ: Prentice Hall, 2003.

[50] Singto S, Supap T, Idem R, et al. Synthesis of new amines for enhanced carbon dioxide (CO_2) capture performance: the effect of chemical structure on equilibrium solubility, cyclic capacity, kinetics of absorption and regeneration, and heats of absorption and regeneration. *Int J Greenh Gas Con* 2013; 167:97–107.

[51] Sanz-Pérez ES, Olivares-Marín M, Arencibia A, et al. CO_2 adsorption performance of amino-functionalized SBA-15 under post-combustion conditions. *Sep Purif Technol* 2016; 17:366–75.

[52] Kim TW, Kleitz F, Paul B, et al. MCM-48-like large mesoporous silicas with tailored pore structure: facile synthesis domain in a ternary triblock copolymer-butanol-water system. *J Am Chem Soc* 2005; 127:7601–10.

[53] Qian L, Ren Y, Liu T, et al. Influence of KIT-6's pore structure on its surface properties evaluated by inverse gas chromatography. *Chem Eng J* 2012; 213:186–94.
[54] Pirez C, Caderon JM, Dacquin JP, et al. Tunable KIT-6 mesoporous sulfonic acid catalysts for fatty acid esterification. *ACS Catal* 2012; 2:1607–14.
[55] Yue MB, Sun LB, Cao Y, et al. Efficient CO_2 capturer derived from as-synthesized MCM-41 modified with amine. *Chemistry* 2008; 14:3442–51.
[56] Zhang X, Qin H, Zheng X, et al. Development of efficient amine-modified mesoporous silica SBA-15 for CO_2 capture. *Mater Res Bull* 2013; 48:3981–6.
[57] Changa FY, Chaoa KJ, Chengb HH, et al. Adsorption of CO_2 onto amine-grafted mesoporous silicas. *Sep Purif Technol* 2009; 70:87–95.
[58] Sanz R, Calleja G, Arencibia A, et al. CO_2 adsorption on branched polyethyleneimine-impregnated mesoporous silica SBA-15. *Appl Surf Sci* 2010; 256:5323–8.
[59] Linneen NN, Pfeffer R, Lin YS. Amine distribution and carbon dioxide sorption performance of amine coated silica aerogel sorbents: effect of synthesis methods. *Ind Eng Chem Res* 2013; 52:14671–9.
[60] Wang L, Yao M, Hu X, et al. Amine-modified ordered mesoporous silica: the effect of pore size on CO_2 capture performance. *Appl Surf Sci* 2015; 324:286–92.
[61] Heydari-Gorji A, Yang Y, Sayari A. Effect of the pore length on CO_2 adsorption over amine-modified mesoporous silicas. *Energy Fuels* 2011; 25:4206–10.
[62] Dao DS, Yamada H, Yogo K. Large-pore mesostructured silica impregnated with blended amines for CO_2 capture. *Ind Eng Chem Res* 2013; 52:13810–7.
[63] Zelenak V, Badanicovaa M, Halamovaa D, et al. Amine modified ordered mesoporous silica: the effect of pore size on CO_2 capture. *Chem Eng J* 2008; 144:336–42.